

## A direct comparison of EMI data and borehole data on a 1000 ha data set



Rasmus Rumph Frederiksen\*, Anders Vest Christiansen, Steen Christensen,  
Keld Rømer Rasmussen

Department of Geoscience, Aarhus University, Høegh-Guldbergs Gade 2, 8000 Aarhus C, Denmark

### ARTICLE INFO

#### Keywords:

Field techniques  
Geophysical methods  
Electromagnetic induction  
Denmark

### ABSTRACT

Increasingly, the frequency domain electromagnetic induction (EMI) method is used to study soil properties and hydrological properties on different scales. Yet, EMI data are most often used as they are or with the low induction number approximation. Moreover, reported studies have been fairly small (< 100 ha) and to our best knowledge quantitative comparisons with boreholes have not been reported. In the present study we collect, process and invert a 1000 ha EMI data set, and we directly compare the EMI data with borehole data. EMI data were collected with a line spacing of 20 m, resulting in approximately 110,000 processed soundings, which were inverted with a full non-linear algorithm. The EMI results were then evaluated against lithological information from 125 boreholes. The results show that with an EMI instrument we can map the shallow (< 6 m) architecture on small-catchment scale (1000s ha) in a complicated glacial sedimentary environment. The mapping of the geological units was evaluated by a quantitative analysis in which we developed a general methodology for directly comparing EMI results and borehole data. After linking geological units to measured resistivities, we found that 103 out of 125 boreholes were reproduced by the EMI results. We attributed the few non-reproducible boreholes to be caused by local scale geological units, abrupt lateral variations in either geology or resistivity, and inaccurate borehole coordinates. We conclude that EMI can provide the architectural input with the necessary detail and quality to characterize areas of up to 1000s ha.

### 1. Introduction

Mapping shallow hydrogeological architecture is important for the assessment of water, nutrient and contaminant exchange between land surface, soil, aquifers, and surface waters (Winter et al., 1998). In farmed catchments this is of particular importance because of the risk of leaching of excess nutrients to aquifers and streams (Kronvang et al., 2005).

The most commonly used methods to map the shallow hydrogeological architecture are drillings and hydrogeophysical methods. It is well known that drillings – core samples in particular – can provide detailed information about the local layering and lithology. However, drillings are point measurements, invasive, expensive, and require dense sampling in order to produce architectural input with the necessary detail and quality to characterize areas of up to catchment scale. Therefore, two decades ago researchers began to realize the importance of applying electromagnetic induction (EMI) in soil mapping (Brus et al., 1992; Knotters et al., 1995). Today EMI is easy to set up, use and mobilize and a number of commercial instruments are available alongside several processing and inversion programs. The use of EMI in agricultural contexts has been reviewed by Corwin and Lesch

(2005) and in soil studies by Doolittle and Brevik (2014).

Several studies have demonstrated how soil properties can be mapped using EMI in combination with soil samples. These studies have mapped the spatial distribution of bulk soil average clay content using EM34 and EM38 instruments (Triantafyllis and Lesch, 2005), delineated the spatial extent of a clay lens using a EM38DD (Cockx et al., 2007), mapped patterns between soils and vegetation using a DUALEM-1S (Robinson et al., 2008), predicted regional-scale soil variability using a EM38 (Harvey and Morgan, 2009), mapped small-scale variations of the depth to the interface in a two-layered soil using EM38DD and DUALEM-21S (Saey et al., 2011, 2012), and modelled the thickness of a compacted soil layer using a EM38-MK2 (Islam et al., 2014). Fewer studies have used EMI data in combination with ancillary data to map soil properties. These studies have characterized a 100 ha hill-slope using an EM38DD instrument and gamma-ray spectroscopy data (Popp et al., 2013) and investigated lateral and vertical changes in soil properties that influence crop performance on field scale using a CMD-MiniExplorer, satellite imagery and ERT transects (Rudolph et al., 2015). However, we are not aware of any studies that have compared EMI data directly with lithological logs from drillings, or have > 100 ha EMI data. In the present study we will make a direct comparison of

\* Corresponding author.

E-mail address: [rasmus.rumph@geo.au.dk](mailto:rasmus.rumph@geo.au.dk) (R.R. Frederiksen).

EMI data and borehole data on a 1000 ha data set (125 boreholes and approximately 1,275,000 raw EMI sounding points).

Increasingly, soil properties are mapped by inverting EMI data. For example, data from a DUALEM-421S instrument have been inverted with the inversion program EM4Soil to model coastal salinity in quasi-2D and -3D (Davies et al., 2015), soil salinization in quasi-3D (Zare et al., 2015), and image electromagnetic apparent conductivity as a proxy for volumetric soil water for an irrigated Lucerne field (Huang et al., 2016), respectively, and EMI data from a CMD-MiniExplorer instrument have been inverted to obtain quasi-3D models of the subsurface (von Hebel et al., 2014). However, Christiansen et al. (2016) showed (1) that dedicated processing of EMI data is necessary to remove coupling from anthropogenic structures (fences, phone cables, paved roads, etc.), and (2) that carrying out a dedicated full non-linear inversion with spatial coherency constraints improves the accuracy of resistivities and structures compared to that obtained by using the data as they are or using the Low Induction Number (LIN) approximation. In the present study we will therefore do both (1) and (2).

We hypothesize that EMI can provide the architectural input with the necessary detail and quality to characterize areas of up to small-catchment scale (1000s ha). The hypothesis was tested by (1) collecting, processing and inverting a 1000 ha EMI data set, and (2) quantitatively comparing EMI data and borehole lithological information from a spatially dense network of boreholes.

## 2. Materials and methods

### 2.1. Study site

The study is carried out within the Knivsbaek catchment (1200 ha, 56°11'N, and 8°61'E) (Fig. 1) which is located in Western Denmark in one of the major west-Danish landscapes – Skovbjerg hill-island. Hill-islands are isolated “islands” of glacial landscape of the Saalian (Illinoian) age which were surrounded by out-wash plains during the Weichselian (Wisconsinan) glaciation (Dalgas, 1867). The topography of the study site is gently undulating and land surface elevation in the study site ranges from around 30 m above sea level in the lower parts of the stream valley and up to 85 m in the hilly parts. The land use is mostly agricultural (> 90%) with grain, corn and grass as main crop types.

Lithological logs from a dense network of boreholes (Fig. 1) indicate that Knivsbaek stream runs in glacial deposits consisting of tills and glacial outwash sand and gravel of Quaternary age on top of alternating layers of Miocene marine, lacustrine, and fluvial deposits (Rasmussen et al., 2010). There are few geological maps available in the study area

(not shown). These are regional scale maps which don't show the local variability needed for the present study. The thickness of the Quaternary deposits varies, but is everywhere < 10 m. Moreover, the Miocene deposits can be divided into low-permeable Mica clay in the western part and high permeable Quartz sand in the eastern part. The shallow geology is chaotic, though – probably due to glacial and periglacial processes.

The present study is a sub-study in an overarching investigation of the groundwater-surface water interaction in the Knivsbaek catchment. From these investigations we know that hydrographs are event-flow dominated by shallow run off – such as surface, interflow and tile drain runoff. Hence, we expect the shallow hydrogeological architecture to strongly influence the runoff – together with the flat topography of low-lying areas where a groundwater table is present at shallow depth.

However, even though the borehole density is high, it is too small to capture the variations in geology. With this in mind, we find the study site ideal for testing and validating the capabilities of EMI data to map shallow hydrogeological architecture – and thereby potentially improve the understanding and quantification of the system.

### 2.2. Borehole data

Danish boreholes are stored in the public Jupiter database (<http://jupiter.geus.dk>) which is maintained by the Geological Survey of Denmark and Greenland (GEUS) (Møller et al., 2009). The Jupiter database contains > 280,000 boreholes with information such as driller's log, UTM coordinates, administrative information (e.g. purpose, use, pumping quantities), geological description, pressure head and geochemical description. Boreholes in the Knivsbaek Catchment have been drilled with two purposes: extraction of water (i.e. for irrigation or drinking water) and lithological investigations (mostly carried out in a campaign looking for Miocene brown coal layers).

Boreholes for the comparison of EMI data and borehole lithological information were selected from the Jupiter database based on two criteria: (1) the borehole purpose should be lithological investigation (referred to as brown coal boreholes); and (2) the boreholes should be within 20 m from the nearest EMI data point. Brown coal boreholes are used for our analysis because they were described by skilled geologists from GEUS which ensures a homogeneous and high quality lithological description, and the majority were auger drilled which ensures lithological log information of high quality. Furthermore, brown coal boreholes were drilled in a dense (250 × 250 m) grid and lithology was described to 15 m depth. Only boreholes within 20 m distance from nearest EMI data point are used because the lateral variation of the shallow hydrogeological architecture is significant.

A total of 125 boreholes (Fig. 1) were used for the analysis. The EMI

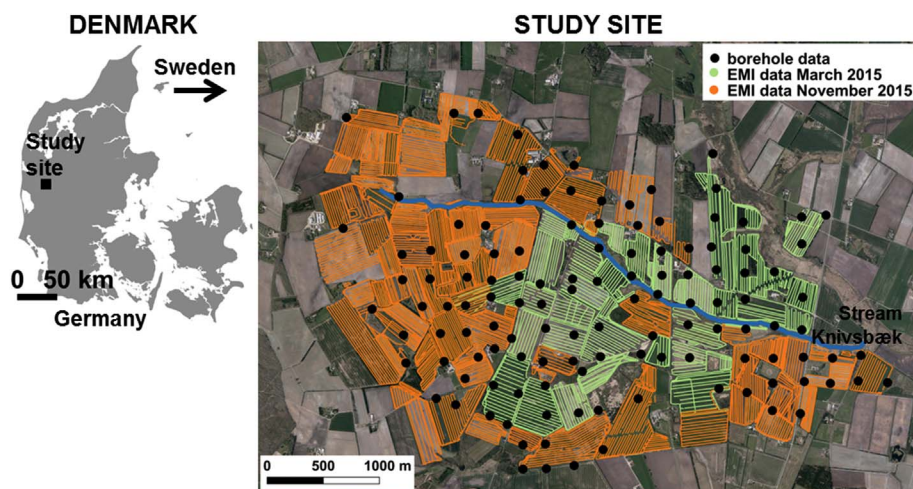


Fig. 1. The study site including borehole data points and EMI data points.

data covers 1000 ha which yields a density of 12.5 boreholes per 100 ha. For comparison, Schamper et al. (2014) had 0.38 boreholes per 100 ha for their qualitative analysis comparing Airborne EM data and boreholes.

### 2.3. Collecting, processing and inverting EMI data

#### 2.3.1. EMI instrument

The EMI instrument used in this study was a DUALEM-421S instrument (DUALEM Inc., Milton, ON, Canada). The instrument has six transmitter-receiver pairs (1-, 2- and 4-m horizontal co-planar (HCP) and 1.1-, 2.1- and 4.1-m perpendicular-planar (PRP)) that operate at a frequency of 9 kHz. Thus, the system simultaneously obtains information about the electrical conductivity (mS/m) of the soil in six different depth ranges (1.5-, 3-, 6-, 0.5-, 1- and 2-m approximate sounding depth, respectively). The variety of configurations with different sampling volumes makes the DUALEM-421S ideal for the investigation of the thickness and electrical conductivity of layering in the top 5–10 m of the subsurface. In wetlands and areas with very shallow clay deposits we found the depth of investigation (DOI, Christiansen and Auken, 2012) to be 3–6 m. In areas with thick sand deposits, the DOI was 8–10 m. The instrument makes a unique measurement ten times per second, while a GPS connected to the system ensures detailed positions of the measurements. The logging of positioning and EMI data are controlled by software developed by the HydroGeophysics Group at Aarhus University (<http://hgg.au.dk/>) which ensures data synchronization and easy in-field data evaluation (Christiansen et al., 2016).

#### 2.3.2. Collecting EMI data

The survey was carried out in two phases with a total of approximately 1000 km survey lines. Phase one of the survey was conducted during three days in mid-March 2015 with changing weather conditions (green dots in Fig. 1). Phase two of the survey was conducted early November 2015 after an October with unusually little precipitation (orange dots in Fig. 1).

The EMI instrument was mounted on a non-metallic sled at a height of 0.285 m above land surface and towed two meters behind a 4WD quad bike. The driving speed during acquisition was 20–25 km/h and the measurement frequency was 10 Hz resulting in a unique measurement every 0.6–0.8 m along survey lines.

Data was collected by driving along wheel tracks, which in Denmark are spaced approximately 20 m on the agricultural fields. In addition, data were collected along the perimeter of each field. The reason is that when turning at the ends of the fields the quad bike comes too close to the instrument, which results in coupled soundings that need to be removed during processing. Inaccessible areas (blank areas in between survey lines in Fig. 1) were due to the presence of vulnerable crops, forest, free standing water, muddy conditions, and/or man-made features (such as fences, phone cables, paved roads, etc.).

At this resolution and speed, it was possible to map approximately 20 ha per hour. For comparison, De Smedt et al. (2013) mapped 0.75 ha per hour – looking for archaeological features and geomorphological variations – and totaling 90 ha.

#### 2.3.3. Processing and inverting EMI data

EMI data need to be processed in order to give the correct information about the subsurface (e.g. Auken et al., 2009a; Christiansen et al., 2016). Before processing, raw EMI data were imported to a database. Every data point was imported and the noise (relative STD) for every data point was set crudely to 1.05 (5%).

EMI data were processed in Aarhus Workbench (Auken et al., 2009b) in two steps. First, a running mean filter of 10 m was applied to the raw-data to increase the signal-to-noise ratio while maintaining all significant geological variations. Following this, the dataset was downsampled to one sounding every 5 m, which again was estimated to retain all relevant structures.

Second, noisy data were cut out. It is well known that man-made features (such as fences, phone cables, paved roads, etc.) induce couplings to EMI data (e.g. Christiansen et al., 2016). Coupled data affect the inversion and could mistakenly be interpreted as anomalous geological units. Therefore an important step in the processing is to cull coupled raw data. In practice, we cull approximately 5 m to both sides of a disturbing element such as fences, phone cables, and paved roads. Our EMI data set consisted of around 1,275,000 raw sounding points which after processing was reduced to around 110,000 1D models, one for every 5 m.

After processing, EMI data were inverted with the inversion code AarhusInv (Auken et al., 2014) which is used extensively for electro-magnetic data, especially airborne (e.g. Mikucki et al., 2015; Podgorski et al., 2015). Each local 1D model has 15 layers with layer thicknesses that increase logarithmically from the first layer boundary at 0.2 m down to the deepest boundary at 12 m. The forward algorithm is a 1D forward solution without approximations (e.g. outlined by Ward and Hohmann, 1988), such as the commonly used low induction number, or LIN. The LIN-approximation is well-suited in high-resistivity environments, but introduces increasingly higher errors at lower resistivities. In Christiansen et al. (2016) numbers are presented on the error introduced by using the LIN-approximation.

For the inversion we used the spatially constrained inversion scheme (SCI) – which is detailed in Viezzoli et al. (2008) – that produces quasi-3D conductivity modelling of electromagnetic data. In short, the SCI is a standard least-squares inversion of a layered earth regularized through spatial constraints ensuring spatially coherent models by migrating information through the constraints. The lateral constraints were set to a factor of 1.600, which roughly means that resistivities of adjacent soundings were allowed to change with up to roughly 60% from sounding to sounding. This is considered fairly loose, which reflects expectations for the lateral geological variations. The vertical constraints on the other hand were set to a factor of 3.000 reflecting fairly abrupt vertical geological variations.

### 2.4. Comparing EMI data and borehole data

In order to compare EMI data and borehole data we had to link geological units to measured resistivities. Numerous studies have done that for Danish sediments. Fig. 2 shows the resistivity ranges found in a highly cited study by Thomsen et al., 2004.

The best-suited lithological boundary for the boreholes was defined as the depth to the top of the first appearing clay layer. The best-suited resistivity boundary for each EMI model was defined as the top of the first layer with a resistivity of  $< 80 \Omega\text{-m}$  (cut-off resistivity) from the top. The chosen cut-off resistivity value is discussed in Section 3.3.

Moreover, two things were simplified: (1) the different geological units in the survey area were reduced to just sand and clay, and (2) the lower depth of the comparison was set to six meters (Depth Of Analysis, DOA). This DOA is chosen to make the comparison consistent throughout the analysis, since the DOI is spatially varying.

The resistivity boundary for each EMI model was extrapolated to borehole locations using the nearest neighbour method with a search radius of 20 m resulting in 125 boreholes with corresponding resistivity boundaries.

Each of these boreholes was assigned to one of four groups: “S +”, “SC +”, “S –” and “SC –” (Fig. 3). If the depth to the lithological boundary was absent or below DOA (i.e. 6 m depth) the borehole was assigned to either “S +” (the depth to resistivity boundary was also absent or below DOA) or “S –” (the depth to the resistivity boundary was above DOA). If the depth to the lithological boundary was above DOA the borehole was assigned to either “SC +” (the depth to the resistivity boundary was also above DOA) or “SC –” (the depth to the resistivity boundary was absent or below DOA). In other words, the two “+” groups agree on having or not having both the lithological boundary and the resistivity boundary above DOA, while the two

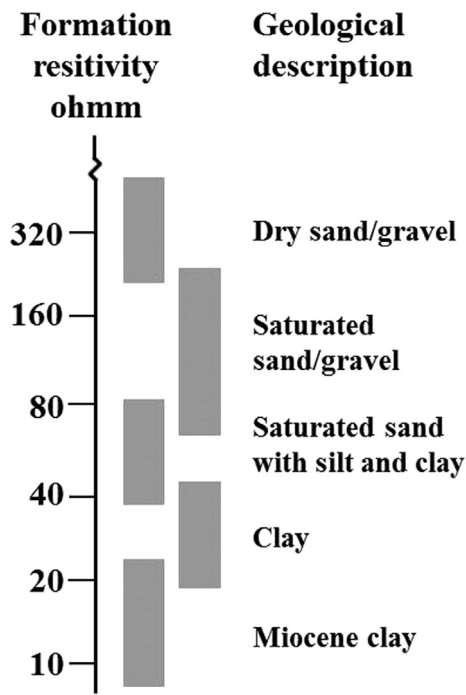


Fig. 2. Resistivity ranges expected for various Danish sediments (modified from Thomsen et al., 2004).

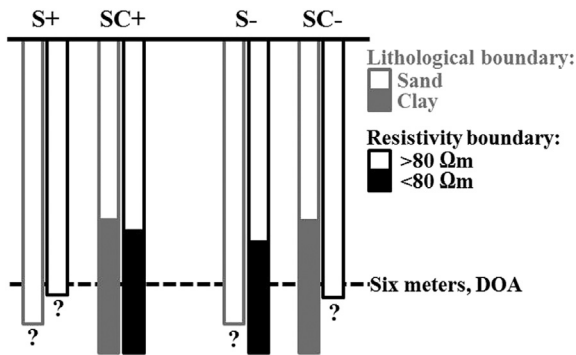


Fig. 3. The boreholes were assigned to one of four groups: “S +”, “SC +”, “S –” and “SC –”.

“–” groups disagree.

### 2.5. Hand drilling selected borehole locations

During our preliminary analysis we identified 27 borehole locations which had a lithological boundary but no resistivity boundary (i.e. “SC –”). In order to investigate whether it was the EMI data or the borehole data that were wrong, we examined 16 of these 27 locations further. The lithological boundary (i.e. clay layer) appeared in different depths in the 27 locations, and the initial idea was to hand drill to identify the boundary. Though, our hand drill equipment had a maximum drilling depth of 3.5 m so we chose to drill only at locations indicating clay no deeper than three meters, which were 16 locations. During a two day field campaign (20–21 September 2016), each of the 16 locations was drilled until either the reported clay deposit was found or the maximum drilling depth was reached. If clay was found, a sample was taken and the resistivity was measured in the laboratory using a Wenner configuration with 1 cm spacing between electrodes. The measured resistivity of the sample was compared to the resistivity measured with EMI. If no clay was found, no lithological boundary was assigned, hence, the borehole was moved from group “SC –” to group “S +” (ten boreholes were moved). The corrected lithological bound-

aries were used for the remaining analysis.

## 3. Results and discussion

### 3.1. EMI inversion results

Fig. 4 shows mean resistivity maps for one meter depth intervals going from the surface to six meters depth. Blue colours correspond to low resistivity values (typically fine-grained sediments with some clay content), green colours correspond to intermediate resistivity values (typically tills and saturated coarse-grained sediments like sand and gravel) and red colours correspond to high resistivity values (typically unsaturated coarse-grained sediments like sand or gravel).

The overall normalized misfit resulting from the inversion is 1.98 indicating that we are not fitting within the assigned noise of 1.05 (5%). The spatial distribution of the misfit (not shown) indicates that the higher misfits are observed in areas with the highest resistivities, i.e. the lowest signals, and this suggests that the assigned noise is too small for these data.

High resistivity values for all depths are observed in the southwest and northeast indicating areas with unsaturated sandy deposits. Low resistivity values are observed from one meter depth in an area going from northwest to south indicating clay sediments below a thin sand layer. In addition to these main patterns, EMI data reveals smaller zones of contrasting resistivity values of which five are highlighted (A, B, C, D and E in Fig. 4) in the following.

Zone A has high resistivity values for all depths and stands out as an anomaly in an otherwise low resistivity area. The mapped part of zone A is 3000 m long and on average 300 m wide – and may continue out of the survey area in the NW- and SE-direction. Zone B also has high resistivity values for all depths but is smaller (150 × 600 m<sup>2</sup> and 60 × 460 m<sup>2</sup>) than zone A. B is fully delineated and could be two small sand filled buried valleys. Zone C (100 × 300 m<sup>2</sup>) has low resistivity values while zone D (240 × 60 m<sup>2</sup>) has low-to-medium resistivity values for all depths. Both C and D stand out as anomalies in an otherwise high resistivity area. C could be a Miocene mica clay lens while D could be Quaternary till or outwash clay deposits. Zone E is larger than the other zones, has low-to-medium resistivities and has diffuse lateral boundaries. This zone could be either peat or till. Peat requires a basin structure (depression), whereas till commonly requires a hill structure. Hence, zone E may be two zones: a western peat zone and an eastern till zone.

### 3.2. Comparing EMI data and borehole data

Fig. 5 shows a plot of the depths to the lithological boundary at the borehole locations on top of a 2D theme map of the depth to the resistivity boundary. It is seen that the lithological and resistivity boundaries match well and that there is no significant pattern in the observed misfits.

Fig. 6 shows a profile with EMI data, borehole data and the resistivity boundary. The variations in the lithology and the resistivity are significant over the length of the section. Along this particular section there are three good crosschecks (B, C and D) and three poor crosschecks (A, E and F). Moreover, it is seen that a range of resistivities could be used as cut-off value.

Fig. 7 shows for the “SC +” boreholes the difference between the depth to the resistivity boundary and the depth to the lithology boundary as a function of the latter. It is seen that most “SC +” boreholes have a lithological (and resistivity) boundary around 0.5–2.5 m depth. Moreover, there is a correlation between the depth to the lithological boundary and the difference between the lithological boundary and the resistivity boundary (gray line in Fig. 7). This indicates that the EMI method overestimates the depth to the lithological boundary for very shallow boundaries, while it underestimates the

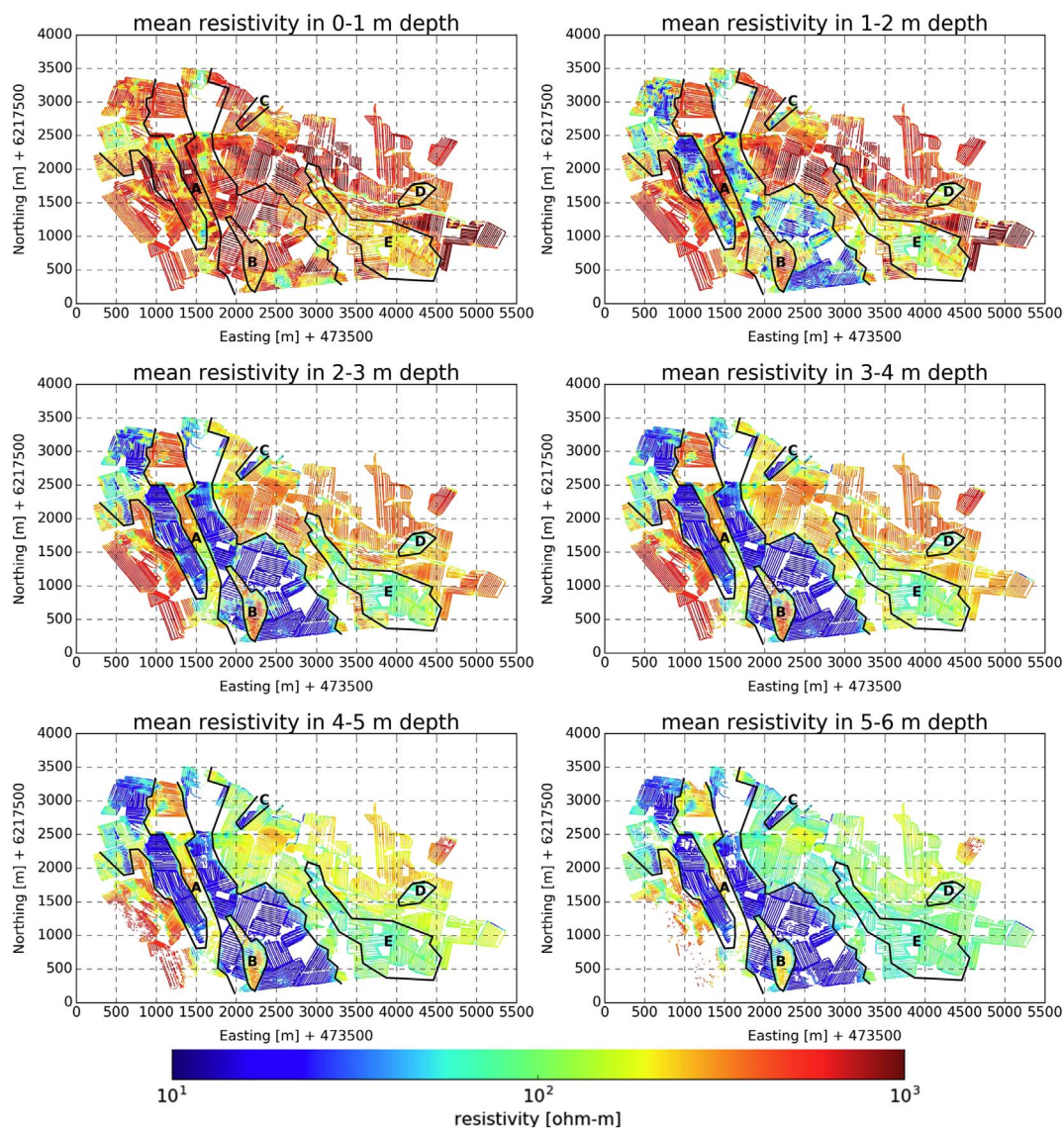


Fig. 4. Mean resistivity maps for one meter depth intervals going from surface to six meters depth. Five zones (A, B, C, D and E) are highlighted and discussed in the main text.

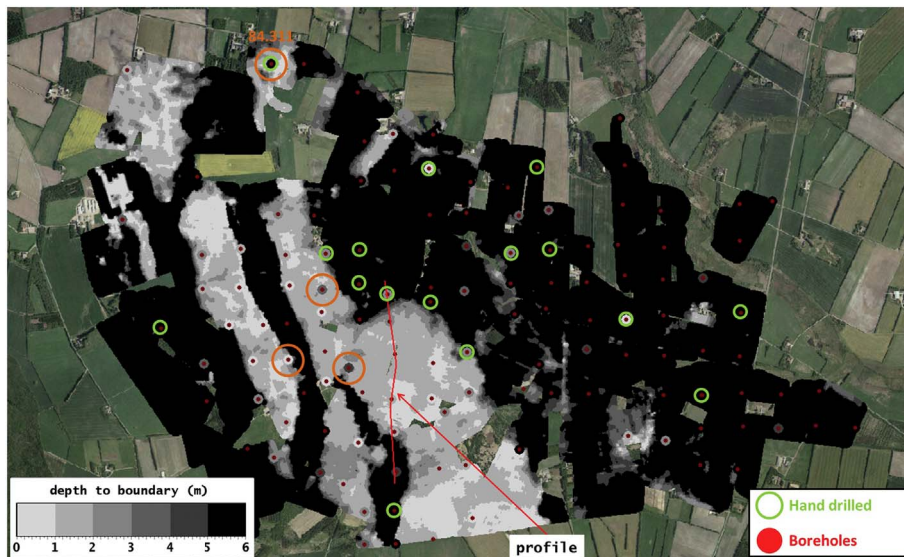


Fig. 5. The depths to the lithological boundary (gray-scale filled circles) and the resistivity boundary (gray-scale 2D theme) results are shown. Locations of hand drilled locations (green circles) and all borehole locations (red dots) are marked. Locations mentioned in the main text (orange circle and number) and profile line are marked as well. (For interpretation of the references to colour in this figure legend, the reader is referred to the web version of this article.)

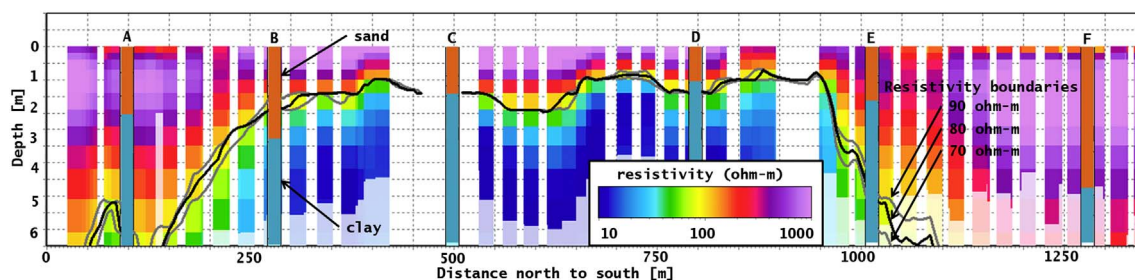


Fig. 6. A profile with EMI data (see colour scale), borehole data (A-F where orange is sand and blue is clay) and three resistivity boundaries (70, 80 and 90 Ω-m) are shown. (For interpretation of the references to colour in this figure legend, the reader is referred to the web version of this article.)

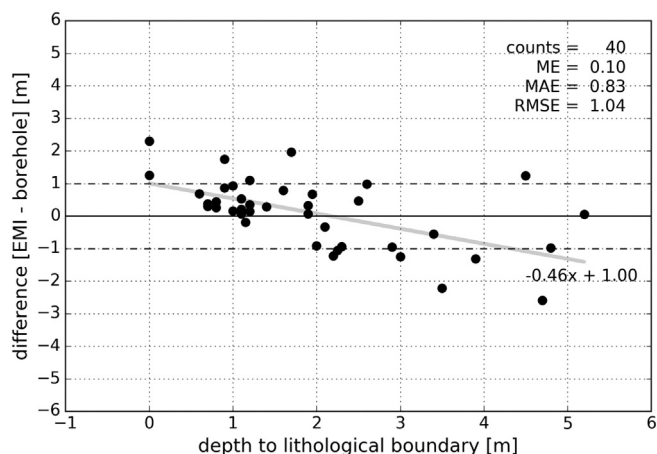


Fig. 7. Difference between the depth to the resistivity boundary and the depth to the lithology boundary as a function of the latter for “SC +” boreholes.

depths for deep boundaries. This trend may be due to the fact that we used a single cut-off resistivity value for all depths which can be too simplistic. However, there is no evidence in the borehole data of depth variations in soil salinity or water content. It should be noted that the DOI is always included in the comparison, such that boreholes with resistivity boundaries deeper than the DOI are not part of the comparison. This will especially be important in low-resistivity areas where the DOI is shallow and the deeper parts of the models cannot be trusted. In addition to the general trend, three out of 40 “SC +” boreholes have an absolute residual of 2 m or more (orange circles without numbers in Fig. 5). One out of these three has a positive residual and two have negative residuals – all are located near an abrupt lateral resistivity boundary (Fig. 5).

Occurrence of small-scale variations in the geology is expected to be the cause for mismatch at three – possible 11 – “SC –” boreholes. Here, the geological variation is expected to be too small to be resolved by the EMI. This limitation could be addressed by decreasing the sounding line distance from 20 m in this study to 10 m or even to 5 m. But a smaller sounding line distance would either increase time and costs or decrease dataset size. The mismatches are characterized by being small isolated areas – such as a single mismatching borehole surrounded by numerous matching boreholes. However, for most small-catchment water resource management objectives these small-scale variations in architecture may be unimportant.

Three out of four “S-” boreholes are located near an abrupt lateral resistivity boundary (Fig. 5). The last “S –” borehole (84.311 and orange circle in Fig. 5) is located in the north-western part of the low resistivity area where the resistivity boundary is at around one meter depth. We hand drilled this location and found unsaturated sand from terrain to around 1 m and saturated sand from there. We measured the resistivity to be 90 Ω-m in the laboratory for a sample of saturated sand taken from 1 m depth. EMI models near the location show 90 Ω-m in 0.7–1 m depth and 75 Ω-m in 1–1.4 m depth. In other words, the low

resistivity values in the area may be due to saturated sand.

In summary:

- 103 out of 125 boreholes are grouped into either “S +” or “SC +”, i.e. only 22 of all boreholes in the comparison disagrees on having or not having both the lithological boundary and the resistivity boundary above or below DOA.
- 28 out of 40 “SC +” boreholes (Fig. 7) have an absolute difference between the lithological boundary and the resistivity boundary < 1.0 m. 35 out of 40 have an absolute difference < 1.5 m. The Mean Absolute Error (MAE) for all 40 “SC +” boreholes is 0.83.
- 5 out of 125 boreholes are categorized as “S –”.
- 17 out of 125 boreholes are categorized as “SC-” when corrected for hand drilling results; 11 out of these 17 “SC –” boreholes have not been hand drilled because the clay layer in the reported boreholes is deeper than the maximum hand drilling depth (i.e. 3.5 m).

### 3.3. Cut-off resistivity value

The cut-off resistivity value was used to set the resistivity boundary as the top of the first layer for each EMI model with a resistivity of less than the cut-off value from the top. Table 1 shows summary statistics for cut-off resistivity values of 60, 70, 80, 90 and 100 Ω-m, respectively. These results show that the depth to the lithological boundary and the depth to the resistivity boundary may be fitted nearly equally well using a range of cut-off resistivity values.

Moreover, in Fig. 6 – that showed a profile with EMI data, borehole data and the resistivity boundary – it was also seen that a range of resistivities could be used as cut-off value as seen in Table 1. In the present study we used a cut-off resistivity value of 80 Ω-m to represent clay because this value had slightly better statistics than the other values. A value of 80 Ω-m is in the high end of those displayed in Fig. 2 (modified from Thomsen et al., 2004). It should be noted that the resistivity values for geological units are always presented as ranges – not single values – and that these ranges are site-specific and likely overlapping between lithologies or units.

Moreover, there is a trade-off when fitting the lithological boundary and the resistivity boundary by using a single site-specific cut-off resistivity value on small-catchment scale (1000s ha) because variables such as soil water content, water table elevation, mineral composition,

Table 1  
Summary statistics for cut-off resistivity values of 60, 70, 80, 90 and 100 Ω-m, respectively.

	60 Ω-m	70 Ω-m	80 Ω-m	90 Ω-m	100 Ω-m
Counts <sup>a</sup>	102	102	103	105	101
ME (m) <sup>b</sup>	0.17	0.03	-0.07	0.02	-0.12
MAE (m) <sup>b</sup>	0.50	0.43	0.43	0.62	0.64
RMSE (m) <sup>b</sup>	1.03	0.80	0.78	1.48	1.45

<sup>a</sup> Counts is the number of boreholes in either “SC +” or “S +” groups.

<sup>b</sup> E is the error between the depth to the resistivity boundary and the depth to the lithological boundary.

geochemical composition and depositional environment will vary between survey sites and within these. For example, a lithological boundary consisting of low resistivity clay (e.g. Miocene mica clay) may best be fitted using a low cut-off value, while a lithological boundary consisting of high resistivity clay (e.g. clayey till) may best be fitted using a higher cut-off value. Therefore, local borehole lithological information is crucial in order to link geological units to measured resistivities, and more boreholes are needed if the lateral variations in the hydrogeological parameters are abrupt and pronounced. For example that could be one to two boreholes within each larger zone with homogeneous resistivities.

### 3.4. Hand drillings

Hand drillings were used to investigate whether it was the EMI data or the borehole data that were off for 16 out of 27 locations which had a lithological boundary but no resistivity boundary (i.e. group “SC –”). Ten out of 16 hand drillings showed no clay within the top 3.5 m. The remaining six boreholes had clay at the same depth as reported in the borehole data. Three of these six are located near an abrupt lateral change in resistivity boundary, while three are scattered in the high resistivity areas.

Potential inaccurate borehole coordinates could cause some mismatches. As mentioned, the boreholes used in the comparison of EMI data and borehole lithological information were drilled in the 1940s in order to locate areas for brown coal mining. At that time the locations were assessed using high resolution (1:20,000) topographical maps in the field – not GPS. On the map a field position was indicated with 1 mm precision (20 m resolution). However, at (a few) locations with poor landmarks the uncertainty may be higher, say, twice this value, i.e. about 50 m.

If we assume an X, Y-uncertainty of maximum 50 m it is not unreasonable to imagine that two drillings – one from the old 1940-campaign and another from our 2016-campaign – to be different. Not least because the new drillings only reached 3.5 m and that glacial and periglacial processes may have disturbed the superficial sediments in the study site.

## 4. Conclusions

We collected, processed and inverted a 1000 ha EMI data set, and we made a direct comparison of the EMI data and borehole lithological information.

We found that EMI is able to map shallow (< 6 m) hydrogeologically relevant architecture on small-catchment scale (1000s ha) in a complicated glacial sedimentary environment. The details revealed in the architecture reveal features on a smaller scale than even very dense borehole data (< 250 m). Overall the depth to the lithological boundary and the depth to the resistivity boundary match well. The few mismatches between EMI data and borehole lithological information might be caused by local scale geological units, abrupt lateral variations in either the geology or the resistivity boundary, and inaccurate borehole coordinates.

We found that 80 Ω-m is the best cut-off resistivity value to link geological units to measured resistivity in our particular survey site. However, a range of cut-off resistivity values could have been used. In addition to being site-specific, we argued that the cut-off value might be spatially varying within sites due to the presence of clay units with alternative resistivities and the presence of alternative soil water content, groundwater table elevation, mineral composition, geochemical composition and depositional environment. Therefore, local borehole lithological information is crucial in order to link geological units to measured resistivities.

Clearly, many similar applications in glacial sedimentary environments in the Northern Hemisphere exist where the task is to determine a clay boundary. However, the hydrogeological characterization might

be more difficult in other regions where for example the lithological contrasts are less extreme electrically, the terrain is steeper, or the soil properties are more variable. This limits the general applicability.

Our recommendations for future EMI small-catchment scale applications are (1) collect the EMI data in consecutive days in order to minimize the effect of temporal varying soil properties and water table elevation, (2) always make a dedicated processing and full non-linear inversion with spatial coherency constraints of the EMI data in order to improve the accuracy of resistivities and structures, (3) first make a preliminary interpretation based solely on the EMI models, (4) then make one to two drillings – to approximately 10 m depth – in each larger zone with fairly uniform lateral resistivities in order to assess the site-specific link between the geological units and the measured resistivities and to assess the degree of variations within the survey site, and (5) make the final interpretation of the local geology.

## Acknowledgements

This research has been carried out under the HOBE (Center for Hydrology) project, funded by the Villum Foundation. We would like to thank Lars Rasmussen for help in the field.

## References

- Auken, E., Christiansen, A.V., Westergaard, J.H., Kirkegaard, C., Foged, N., Viezzoli, A., 2009a. An integrated processing scheme for high-resolution airborne electromagnetic surveys, the SkyTEM system. *Explor. Geophys.* 40, 184–192.
- Auken, E., Viezzoli, A., Christensen, A., 2009b. A single software for processing, inversion, and presentation of AEM data of different systems: the Aarhus Workbench. *ASEG Ext. Abstr.* 1, 1–5.
- Auken, E., Christiansen, A.V., Kirkegaard, C., Fiandaca, G., Schamper, C., Behroozmand, A.A., Binley, A., Nielsen, E., Effersø, F., Christensen, N.B., et al., 2014. An overview of a highly versatile forward and stable inverse algorithm for airborne, ground-based and borehole electromagnetic and electric data. *Explor. Geophys.* 46, 223–235.
- Brus, D.J., Knotters, M., van Dooremolen, W.A., van Kernebeek, P., van Seeters, R.J.M., 1992. The use of electromagnetic measurements of apparent soil electrical conductivity to predict the boulder clay depth. *Geoderma* 55, 79–93. [http://dx.doi.org/10.1016/0016-7061\(92\)90006-S](http://dx.doi.org/10.1016/0016-7061(92)90006-S).
- Christiansen, A.V., Auken, E., 2012. A global measure for depth of investigation. *Geophysics* 77, WB171–WB177. <http://dx.doi.org/10.1190/geo2011-0393.1>.
- Christiansen, A.V., Pedersen, J.B., Auken, E., Søe, N.E., Holst, M.K., Christiansen, S.M., 2016. Improved geoarchaeological mapping with electromagnetic induction instruments from dedicated processing and inversion. *Remote Sens.* 8, 1022.
- Cockx, L., van Meirvenne, M., de Vos, B., 2007. Using the EM38DD soil sensor to delineate clay lenses in a sandy forest soil. *Soil Sci. Soc. Am. J.* 71, 1314–1322. <http://dx.doi.org/10.2136/sssaj2006.0323>.
- Corwin, D.L., Lesch, S.M., 2005. Apparent soil electrical conductivity measurements in agriculture. *Comput. Electron. Agric.* 46, 11–43. <http://dx.doi.org/10.1016/j.compag.2004.10.005>.
- Dalgas, E., 1867. *Geografiske billeder fra Heden* (H. 1 & 2).
- Davies, G., Huang, J., Monteiro Santos, F.A., Triantafyllis, J., 2015. Modeling coastal salinity in quasi 2D and 3D using a DUALEM-421 and inversion software. *Groundwater* 53, 424–431. <http://dx.doi.org/10.1111/gwat.12231>.
- De Smedt, P., Saey, T., Lehouck, A., Stichelbaut, B., Meerschman, E., Islam, M.M., Van De Vijver, E., Van Meirvenne, M., 2013. Exploring the potential of multi-receiver EMI survey for geoarchaeological prospecting: a 90 ha dataset. *Geoderma* 199, 30–36. <http://dx.doi.org/10.1016/j.geoderma.2012.07.019>.
- Doolittle, J.A., Brevik, E.C., 2014. The use of electromagnetic induction techniques in soils studies. *Geoderma* 223–225, 33–45. <http://dx.doi.org/10.1016/j.geoderma.2014.01.027>.
- Harvey, O.R., Morgan, C.L.S., 2009. Predicting regional-scale soil variability using a single calibrated apparent soil electrical conductivity model. *Soil Sci. Soc. Am. J.* 73, 164–169. <http://dx.doi.org/10.2136/sssaj2008.0074>.
- von Helber, C., Rudolph, S., Mester, A., Huisman, J.A., Kumbhar, P., Vereecken, H., van der Kruk, J., 2014. Three-dimensional imaging of subsurface structural patterns using quantitative large-scale multiconfiguration electromagnetic induction data. *Water Resour. Res.* 2732–2748. <http://dx.doi.org/10.1002/2012WR013085>. Received.
- Huang, J., Scudiero, E., Choo, H., Corwin, D.L., Triantafyllis, J., 2016. Mapping soil moisture across an irrigated field using electromagnetic conductivity imaging. *Agric. Water Manag.* 163, 285–294. <http://dx.doi.org/10.1016/j.agwat.2015.09.003>.
- Islam, M.M., Saey, T., De Smedt, P., Van De Vijver, E., Delefortrie, S., Van Meirvenne, M., 2014. Modeling within field variation of the compaction layer in a paddy rice field using a proximal soil sensing system. *Soil Use Manag.* 30, 99–108. <http://dx.doi.org/10.1111/sum.12098>.
- Knotters, M., Brus, D.J., Oude Voshaar, J.H., 1995. A comparison of kriging, co-kriging and kriging combined with regression for spatial interpolation of horizon depth with censored observations. *Geoderma* 67, 227–246. [http://dx.doi.org/10.1016/0016-7061\(95\)00011-C](http://dx.doi.org/10.1016/0016-7061(95)00011-C).

- Kronvang, B., Jeppesen, E., Conley, D.J., Søndergaard, M., Larsen, S.E., Ovesen, N.B., Carstensen, J., 2005. Nutrient pressures and ecological responses to nutrient loading reductions in Danish streams, lakes and coastal waters. *J. Hydrol.* 304, 274–288.
- Mikucki, J.A., Auken, E., Tulaczyk, S., Virginia, R.A., Schamper, C., Sørensen, K.I., Doran, P.T., Dugan, H., Foley, N., 2015. Deep groundwater and potential subsurface habitats beneath an Antarctic dry valley. *Nat. Commun.* 6.
- Møller, I., Søndergaard, V.H., Jørgensen, F., Auken, E., Christiansen, A.V., 2009. Integrated management and utilization of hydrogeophysical data on a national scale. *Near Surf. Geophys.* 7, 647–659.
- Podgorski, J.E., Green, A.G., Kalscheuer, T., Kinzelbach, W.K.H., Horstmeyer, H., Maurer, H., Rabenstein, L., Doetsch, J., Auken, E., Ngwisanyi, T., et al., 2015. Integrated interpretation of helicopter and ground-based geophysical data recorded within the Okavango Delta, Botswana. *J. Appl. Geophys.* 114, 52–67.
- Popp, S., Altdorff, D., Dietrich, P., 2013. Assessment of shallow subsurface characterisation with non-invasive geophysical methods at the intermediate hill-slope scale. *Hydrol. Earth Syst. Sci.* 17, 1297–1307. <http://dx.doi.org/10.5194/hess-17-1297-2013>.
- Rasmussen, E.S., Dybkjær, K., Piasecki, S., 2010. Lithostratigraphy of the Upper Oligocene – Miocene succession of Denmark. *Geol. Surv. Denm. Greenl. Bull.* 22, 92.
- Robinson, D.A., Abdu, H., Jones, S.B., Seyfried, M., Lebron, I., Knight, R., 2008. Eco-geophysical imaging of watershed-scale soil patterns links with plant community spatial patterns. *Vadose Zone J.* 7, 1132–1138. <http://dx.doi.org/10.2136/vzj2008.0101>.
- Rudolph, S., van der Kruk, J., von Hebel, C., Ali, M., Herbst, M., Montzka, C., Pätzold, S., Robinson, D.A., Vereecken, H., Weiermüller, L., 2015. Linking satellite derived LAI patterns with subsoil heterogeneity using large-scale ground-based electromagnetic induction measurements. *Geoderma* 241–242, 262–271. <http://dx.doi.org/10.1016/j.geoderma.2014.11.015>.
- Saey, T., Van Meirvenne, M., De Smedt, P., Cockx, L., Meerschman, E., Islam, M.M., Meeuws, F., 2011. Mapping depth-to-clay using fitted multiple depth response curves of a proximal EMI sensor. *Geoderma* 162, 151–158. <http://dx.doi.org/10.1016/j.geoderma.2011.01.015>.
- Saey, T., De Smedt, P., Islam, M.M., Meerschman, E., Van De Vijver, E., Lehouck, A., Van Meirvenne, M., 2012. Depth slicing of multi-receiver EMI measurements to enhance the delineation of contrasting subsoil features. *Geoderma* 189–190, 514–521. <http://dx.doi.org/10.1016/j.geoderma.2012.06.010>.
- Schamper, C., Jørgensen, F., Auken, E., Effersø, F., 2014. Case history assessment of near-surface mapping capabilities by airborne transient electromagnetic data — an extensive comparison to conventional borehole data. *Geophysics* 79, B187–B199.
- Thomsen, R., Søndergaard, V.H., Sørensen, K.I., 2004. Hydrogeological mapping as a basis for establishing site-specific groundwater protection zones in Denmark. *Hydrogeol. J.* 12, 550–562. <http://dx.doi.org/10.1007/s10040-004-0345-1>.
- Triantafyllis, J., Lesch, S.M., 2005. Mapping clay content variation using electromagnetic induction techniques. *Comput. Electron. Agric.* 46, 203–237. <http://dx.doi.org/10.1016/j.compag.2004.11.006>.
- Viezzoli, A., Christiansen, A.V., Auken, E., Sørensen, K., 2008. Quasi-3D modeling of airborne TEM data by spatially constrained inversion. *Geophysics* 73, F105–F113.
- Ward, S.H., Hohmann, G.W., 1988. *Electromagnetic theory for geophysical applications*. Electromagn. Methods Appl. Geophys.
- Winter, T.C., Harvey, J.W., Franke, O.L., Alley, W.M., 1998. *Ground water and surface water: a single resource*. U.S. Geol. Surv.
- Zare, E., Huang, J., Monteiro Santos, F.A., Triantafyllis, J., 2015. Mapping salinity in three dimensions using a DUALEM-421 and electromagnetic inversion software. *Soil Sci. Soc. Am. J.* 79, 1729–1740. <http://dx.doi.org/10.2136/sssaj2015.06.0238>.